

## Article

# Investigation of the Microstructure and Properties of CoCrFeNiMo High-Entropy Alloy Coating Prepared through High-Speed Laser Cladding

Qi Zhang, Meiyang Li, Qin Wang, Fuhao Qi, Mengkai Kong and Bin Han \*

School of Materials Science and Engineering, China University of Petroleum (East China), 66 Chang Jiang West Road, Qingdao 266580, China; zq18353248786@163.com (Q.Z.); lmy\_102411@163.com (M.L.); sdkjdxwq2022@163.com (Q.W.); tuanzi121380221@163.com (F.Q.); kongmkkmk@163.com (M.K.)

\* Correspondence: hbzjh@upc.edu.cn; Tel.: +0532-86983771

**Abstract:** High-speed laser cladding was introduced to prepare a CoCrFeNiMo high-entropy alloy (HEA) coating. The microstructure, composition distribution, micromechanical properties, and corrosion resistance of the CoCrFeNiMo coating were characterized. As a result, the coating exhibited a dual FCC- and BCC-phase structure, and the grain size of the coating prepared through high-speed laser cladding was only 2~5  $\mu\text{m}$ . The upper and lower parts of the coating were composed of equiaxed cellular crystals and slender columnar crystals, respectively. The interdendritic structure was a Mo-rich phase that was distributed in a network-like pattern. The nanoindentation tests revealed that the interdendritic BCC phase had high hardness and an elastic modulus as well as excellent resistance to deformation, while the intradendritic FCC phase possessed superior crack propagation resistance. In addition, the two phases could generate cooperative elastic deformation during the elastic deformation stage. The electrochemical performance of the coating was tested in 3.5 wt% NaCl solution, and the corrosion potential  $E_{\text{corr}}$  and corrosion current density  $I_{\text{corr}}$  of the coating were  $-0.362\text{ V}$  and  $3.69 \times 10^{-6}\text{ A/cm}^2$ , respectively. The high-speed laser cladding CoCrFeNiMo HEA coating had excellent corrosion resistance thanks to the presence of the easily passivating element Mo and grain refinement.



**Citation:** Zhang, Q.; Li, M.; Wang, Q.; Qi, F.; Kong, M.; Han, B. Investigation of the Microstructure and Properties of CoCrFeNiMo High-Entropy Alloy Coating Prepared through High-Speed Laser Cladding. *Coatings* **2023**, *13*, 1211. <https://doi.org/10.3390/coatings13071211>

Academic Editor: Frederic Sanchette

Received: 26 May 2023

Revised: 23 June 2023

Accepted: 29 June 2023

Published: 6 July 2023



**Copyright:** © 2023 by the authors. Licensee MDPI, Basel, Switzerland. This article is an open access article distributed under the terms and conditions of the Creative Commons Attribution (CC BY) license (<https://creativecommons.org/licenses/by/4.0/>).

**Keywords:** high-speed laser cladding; CoCrFeNiMo high-entropy alloy; microstructure; mechanical properties; corrosion resistance

## 1. Introduction

High-entropy alloys typically consist of five or more principal elements in equal or near-equal atomic ratios. The high-entropy effect of multiple principal elements facilitates the formation of a simple solid solution phase structure [1]. The lattice distortion effect enhances their strength [2], and the hysteresis diffusion effect allows them to retain a high strength even at higher temperatures [3]. The properties of high-entropy alloys are compounded by combining the properties of elements, which has the “cocktail” effect [4], resulting in a synergistic effect. A large number of high-entropy alloys can be formed by adding metal elements X (such as Al, Ti, Mo, Si, B, etc.) with significantly different physical and chemical properties to the transition metal CoCrFeNi as the base, and they have been widely studied. Among them, CoCrFeNiMo high-entropy alloys have high resistance to fatigue crack extension [5], while the presence of an FCC matrix and hard intermetallic compounds formed by Mo with Fe, Co, and Ni gives them good overall mechanical properties [6–8]. Zhang et al. [9] adopted an annealing treatment to a CoCrFeNiMo high-entropy alloy prepared through hot isostatic pressing, which can lead to a large amount of  $\mu$  phase inside and can further improve its compressive strength and inhibit cracking. Wu et al. [10] formed a CoCrFeNiMo high-entropy alloy with a denser structure through magnetic levitation melting technology, and, due to the presence of Ni, Cr, and Mo elements,

it has excellent high-temperature wear resistance. An ultrafine lamellar eutectic structure was formed in a CoCrFeNiMo alloy prepared through directional energy deposition (DED), and the strengthening effect was remarkable [11].

A CoCrFeNiMo block high-entropy alloy was initially obtained through vacuum melting, and the obtained alloy has high strength and good corrosion resistance [12]. Sigrun N. Karlsdottir et al. [13] found that the bulk CoCrFeNiMo high-entropy alloy material has high hardness (593 HV) and a low corrosion rate (0.0072 mm/year) and that it has the corrosion resistance required for harsh thermal environments. Andri Isak Thorhallsson [14] and Loana CSÁKI [15] have both demonstrated that CoCrNiFeMo high-entropy alloys can be considered as candidate materials for corrosive thermal environments. Nevertheless, the considerable preparation cost of high-entropy alloy materials impedes their widespread utilization in bulk form. To address this issue, we propose combining surface coating technology with high-entropy alloys, which can fulfill the performance requirements of component surfaces while reducing the application cost of the material.

Laser cladding technology has the characteristics of rapid cooling and rapid heating and can use a high-energy-density laser beam to achieve the rapid melting of powder materials and metallurgical bonding with the substrate, and the coating thickness can be controlled. In the laser cladding process, atoms of various sizes in the CoCrFeNiMo high-entropy alloy system fuse and interact with each other, resulting in lattice distortion and the formation of a second-phase precipitate, thus bringing about solid solution strengthening and precipitation strengthening [16,17]. Deng et al. [18] prepared a CoCrFeNiMo<sub>0.2</sub> high-entropy alloy coating on the TC4 surface, which featured a uniform dendritic microstructure and exhibited improved hardness, oxidation resistance, and corrosion resistance compared to the TC4 substrate. Qiu et al. [19] laser-cladded a CoCrFeNiMo alloy on the surface of a 45 steel substrate, which was strengthened through fine-grained and second-phase reinforcement, resulting in the coating having a higher strength. In addition, with an increase in the scanning speed, the microstructure was refined, and the hardness was improved.

In order to enhance the forming efficiency and to optimize the microstructure and performance of the laser cladding coating, high-speed laser cladding technology has been innovatively developed [20–22]. High-speed laser cladding can adjust the positions of the powder focus and the laser focus so that the cladding powder melts at the intersection of the substrate and the laser beam. Most of the laser energy is directly applied to the powder, significantly reducing the heat input to the substrate and thus enhancing the cladding efficiency and powder utilization. This poses a great challenge to traditional thermal spraying technology. Currently, research on the high-speed laser cladding of high-entropy alloys is relatively limited, focusing mainly on improving the metal microstructure and enhancing the mechanical properties of the coating. Chong et al. [23] utilized high-speed laser cladding technology to prepare an AlCoCrFeNi high-entropy alloy coating on the surface of AISI 1045 steel, which significantly improved the cladding efficiency and processing quality as well as the microhardness and corrosion resistance. A CoCrFeNiMo high-entropy alloy is an alloy system that possesses comprehensive properties [24]. Ma et al. [25] prepared the CoCrFeNiMo<sub>0.2</sub> coating through high-speed laser cladding and compared the microstructure and properties with the traditional laser cladding coating. The results showed that the high-speed laser cladding coating had a fine microstructure and better corrosion resistance. However, the coating was relatively thin, only 360  $\mu\text{m}$ , and it may be difficult to meet the industrial service conditions of a heavy load impact after surface grinding and polishing. As of now, there is little research that has been conducted on the high-speed laser cladding of CoCrFeNiMo high-entropy alloys, especially on the micromechanical properties and corrosion resistance of a CoCrFeNiMo high-speed laser cladding coating.

In this paper, a CoCrFeNiMo high-entropy alloy coating with a thickness in millimeters was prepared through high-speed laser cladding, and its microstructure, phase composition, micromechanical properties, and electrochemical corrosion properties were studied. The correlation between the microstructure and properties of the high-speed laser

cladding CoCrFeNiMo coating was explored to enrich the theoretical basis for the formation of high-entropy alloy coatings, accelerating the industrial application of high-entropy alloy coatings.

## 2. Experimental Materials and Methods

### 2.1. Materials and Methods

CoCrFeNiMo-atomized powder purchased from the manufacturer (Jiangsu Vilory Advanced Materials Technology Co., Ltd., Xuzhou, China) was selected as the cladding powder with the particle size of 15~53  $\mu\text{m}$ . The powder was obtained by melting the five kinds of elemental powders under vacuum ( $\sim 8$  Pa) and high temperature (discharge temperature  $\sim 1630$  °C) and then breaking and solidifying them into spherical particles in a high-purity argon atmosphere (with a purity of 99.999%). The spherical powder produced in this way could fully meet the technical requirements of high-speed laser cladding and coaxial powder feeding. A ZKZM-4000 W optical fiber high-speed cladding laser (Zhongke Zhongmei Laser Technology Co., Ltd, Xi'an, China) was used to manufacture CoCrFeNiMo coating on Q235 plate. The surface of Q235 plate was sanded with sandpaper and cleaned with acetone. The laser spot was a circle with a diameter of 2 mm. The parameters used in the experiment are presented in Table 1.

**Table 1.** Process parameters of high-speed laser cladding.

Power (W)	Cladding Speed (m/min)	Powder Feed Rate (g/min)	Overlap Ratio
1800	3	12	75%

### 2.2. Microstructure and Property Characterization

The surface of the cladding layer to be observed was polished with 600 #~2000 # abrasive paper and then was polished with diamond abrasive paste. The polished samples were used for the characterization and analysis of X-ray Diffraction (XRD), mechanical properties, and corrosion resistance. When observing the microstructure of the coating, it was necessary to use aqua regia ( $\text{HNO}_3$ :  $\text{HCl}$  = 1:3) to corrode the polished surface.

A thermal field emission scanning electron microscope (JEOL JSM-7200F, JEOL, Tokyo, Japan) equipped with energy dispersive spectroscopy (EDS) and backscattered electron (BSE) receiver was utilized to observe the microstructure of the coating. The phase of the coating was characterized through X-ray diffraction (X'Pert PRO MPD, Malvern Panalytical, Malvern, UK). The scanning voltage and current were 40 kV and 40 mA, respectively. A scanning speed of  $0.3^\circ/\text{s}$  was used to scan from  $20^\circ$  to  $100^\circ$  in continuous mode. The micromechanical properties of high-speed laser cladding CoCrFeNiMo HEA coating were conducted by using HYSITRON TI PREMIER Nanoindenter (Bruker, Billerica, MA, USA). The loading process involved a loading time of 10 s followed by a holding period of 2 s and a final unloading time of 5 s. We formed a 3-row 10-column nanoindentation dot matrix with loading range from 5000  $\mu\text{N}$  to 500  $\mu\text{N}$ . The loading pressure decreased by 500  $\mu\text{N}$  from left to right, and the maximum loading pressure of the same column was equal. The CS310 electrochemical workstation, equipped with a three-electrode system, was employed to evaluate the electrochemical corrosion resistance of the high-entropy alloy coating in a 3.5 wt% NaCl solution. We used a coating sample as the working electrode, a platinum plate as the auxiliary electrode, and a calomel electrode as the reference electrode. The electrochemical impedance of the system was tested at the open-circuit potential, and the test frequency range was  $10^{-2}$  Hz~ $10^5$  Hz. The scanning rate of the potentiodynamic polarization test was 1 mV/s, and the scanning potential range was from  $-0.5$  V (vs. EOCp) to 1.5 V (vs. EOCp). Finally, we observed the corrosion morphology through SEM. We repeated the above tests three times to ensure the reliability of the experimental results.

### 3. Results and Discussion

#### 3.1. Microstructure Analysis

Figure 1 shows the BSE morphology and its EDS mapping of the high-speed laser cladding CoCrFeNiMo HEA coating, whose surface was polished and uncorroded. The polished surface of the coating was not corroded by the pickling solution, and the backscattered electron image showed the equiaxed grain morphology, indicating that there must be element segregation inside and outside of the grain of the coating. According to mapping, Mo exhibited significant segregation in dendritic crystals. Therefore, a microarea composition analysis was conducted on the inside and outside of the dendrites, and the results are shown in Table 2. The results of the microarea composition analysis are in line with the elemental distribution observed during mapping. The four elements of CoCrFeNi were distributed evenly throughout the coating, with Mo being enriched in the interdendritic microarea. It is noteworthy that the atomic mass of Fe was obviously higher than that of the other four elements, mainly due to the melting of the substrate during the laser cladding process, resulting in the Fe atoms entering the coating.

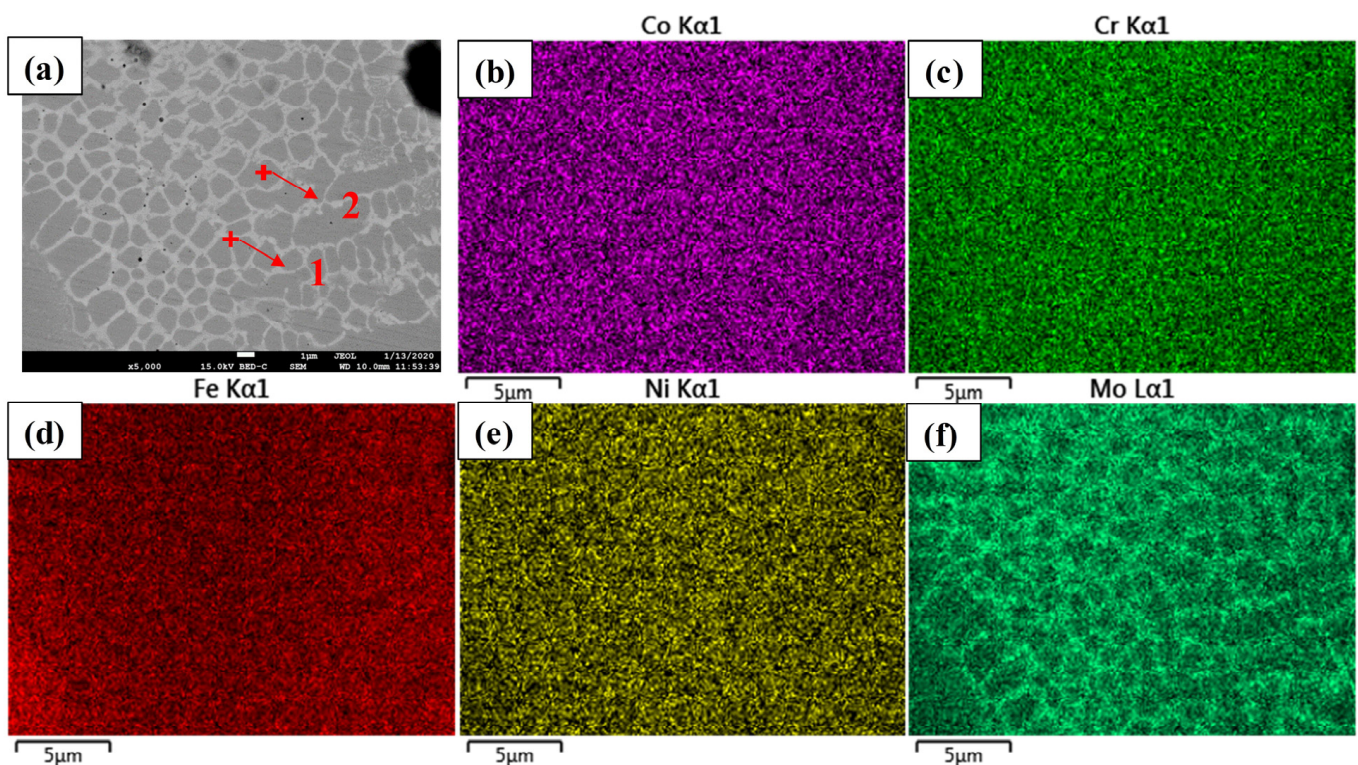


**Figure 1.** BSE image (a) and EDS mapping (b–f) of the CoCrFeNiMo coating on the surface.

**Table 2.** Composition analysis results of dendrite and interdendritic microarea in Figure 1a.

Elements	Co	Cr	Fe	Ni	Mo
Point 1	15.80%	16.10%	33.90%	15.20%	19.00%
Point 2	17.20%	16.20%	34.30%	17.60%	14.70%

The surface microstructure of the CoCrFeNiMo HEA coating is shown in Figure 2. The overlapping areas were prone to corrosion due to element burning and increased tensile stress after remelting. The surface morphology of the coating after corrosion was consistent with the BSE image. There were two types of coating dendritic morphologies: equiaxed cellular crystals and slender columnar dendrites. The Mo-rich structure jointed in a network between the dendrites. According to the ruler in the picture, the size of the equiaxed cellular crystals was very small, only 2~5  $\mu\text{m}$  and the width of the slender

columnar crystal arms was only 2  $\mu\text{m}$ . High-speed laser cladding technology can be utilized to prepare CoCrFeNiMo high-entropy alloy coatings with fine grains.

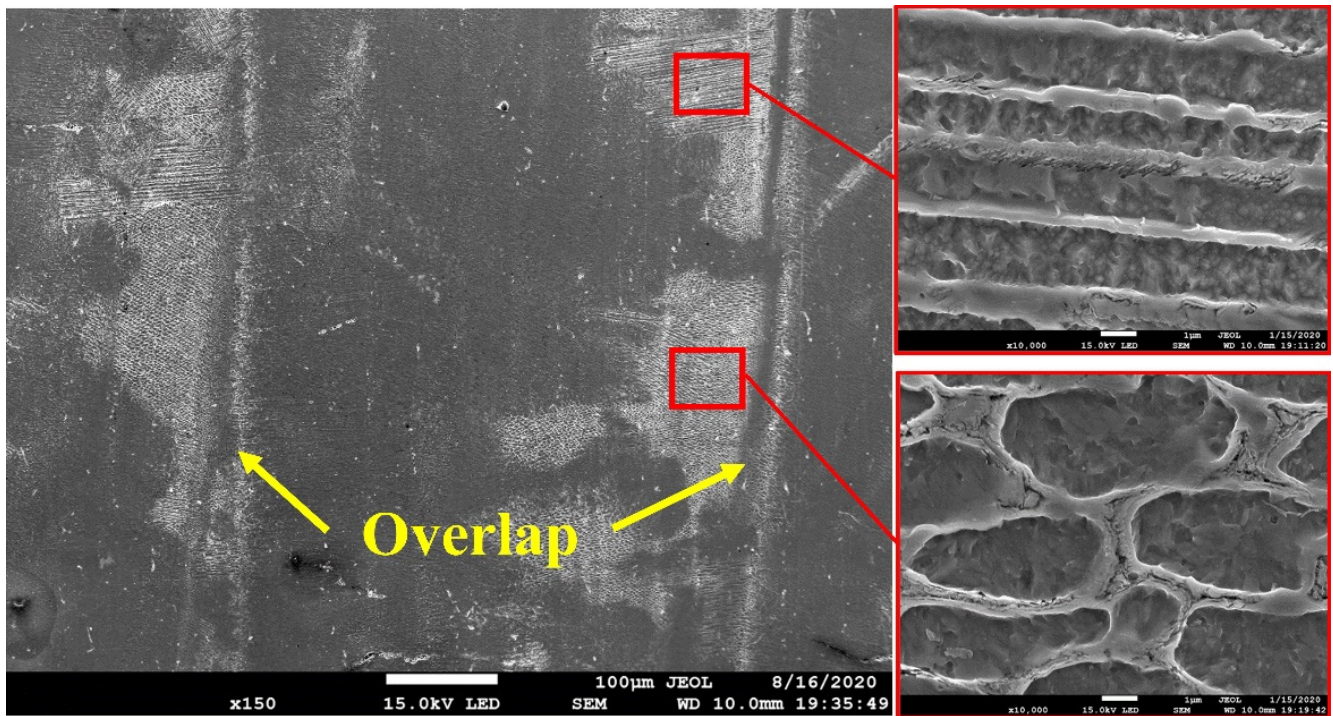


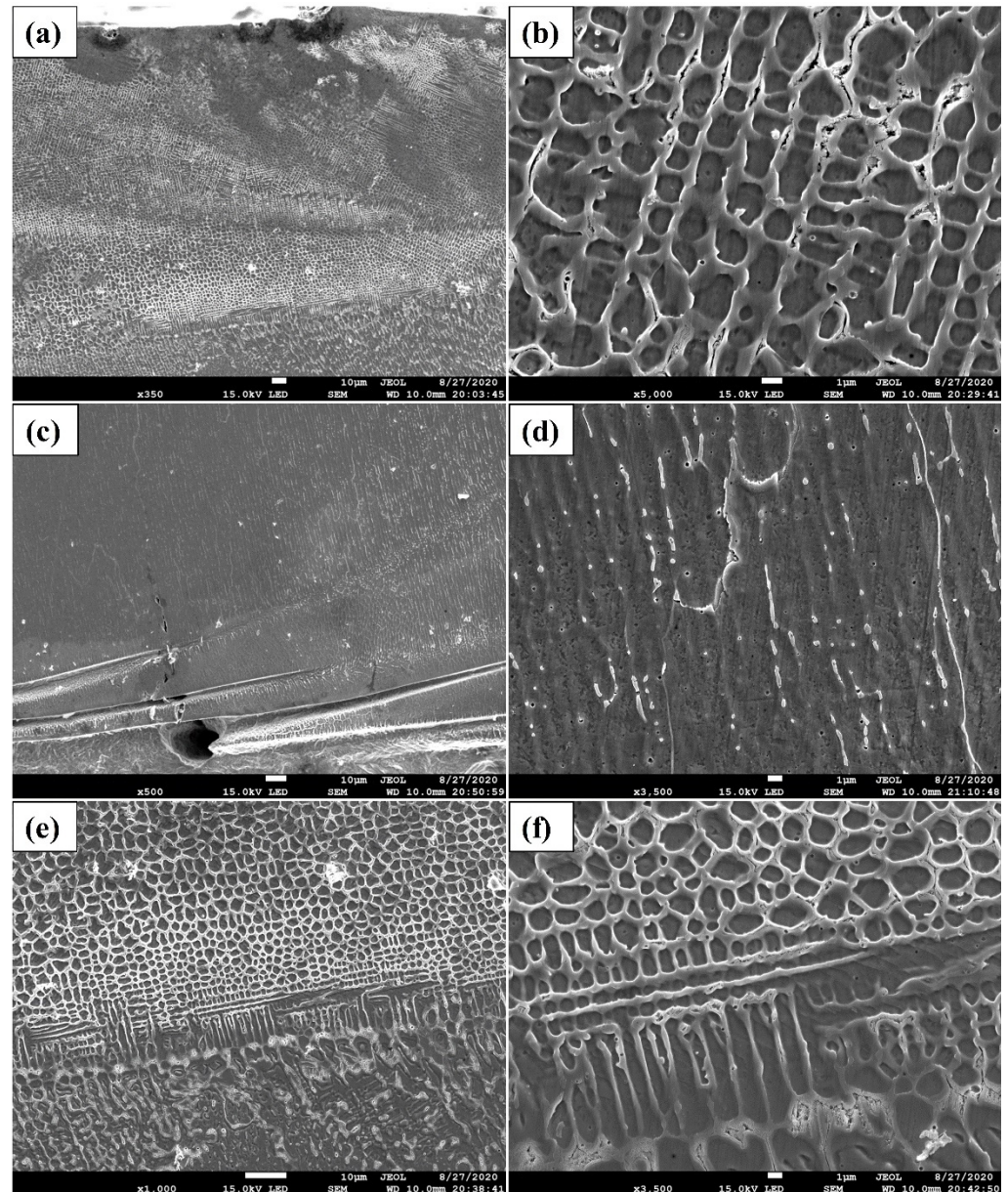
Figure 2. Surface microstructure of the CoCrFeNiMo coating.

Figure 3 shows the microstructure of the cross-section of the high-speed laser cladding CoCrFeNiMo coating. As shown in Figure 3a, the equiaxed cellular crystal morphology was observed in the upper region, while the slender columnar morphology was observed in the lower region as illustrated in Figure 3b. The growth direction was found to be perpendicular to the bottom of the coating, which was mainly attributed to the direction of the heat dissipation of the melt pool. Figure 3e,f are the junctions of the upper and lower parts, where the change in grain morphology can be observed. Closer to the bottom area, the grains were stretched longitudinally. In the cladding process, the temperature gradient at the bottom of the molten pool was large, and the solidification rate was small; therefore, planar crystals were formed at the bonding line. As the liquid–solid interface continued to advance into the molten pool, the solidification rate increased rapidly, and the temperature gradient gradually decreased. The coating was formed from bottom to top in the sequence of planar, cellular, and equiaxed crystals. High-speed laser cladding has a faster cooling speed and higher unidirectional heat dissipation efficiency than traditional laser cladding. Therefore, the process of releasing latent heat into the liquid phase on both sides during axial crystal growth was suppressed, avoiding the generation of secondary dendrites.

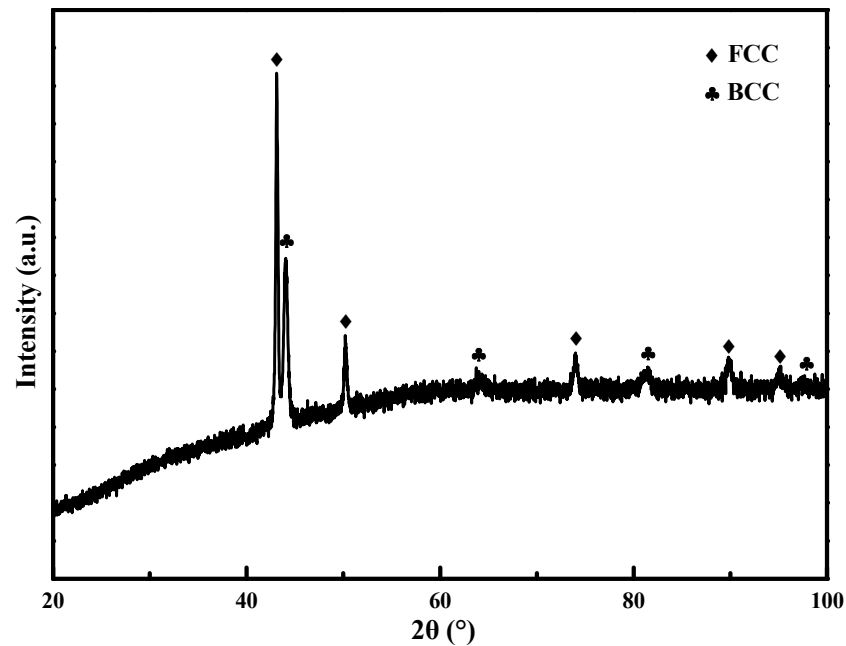
### 3.2. Phase Analysis

Figure 4 is the XRD pattern of the high-speed laser cladding CoCrFeNiMo coating. According to the analysis, the coating consisted of FCC- and BCC-phase structures, which corresponded to the two structures inside and outside of the dendrite in the coating microstructure. The size of the Mo atom itself was larger than that of the other four atoms if the four elements of CoCrFeNi were treated as an element whose phase structure was a single FCC [26]. Under the nonequilibrium solidification conditions of high-speed laser cladding, some Mo atoms could be substitutionally dissolved in the FCC lattice, inducing solid solution strengthening. Nonetheless, due to the differences in chemical properties, such as the electronegativity of the Mo atoms, more of them precipitated between the dendrites, forming intermetallic compounds. The peak strength of the two phases indicates

that the content of the FCC phase was higher than that of BCC. To a certain degree, it can be deduced that the intragranular structure was an FCC phase, and the interdendritic Mo-rich structure was a BCC phase with a better corrosion resistance owing to its high Mo content.



**Figure 3.** Cross-sectional microstructure of the CoCrFeNiMo coating. (a) The upper half area of the coating; (b) local high-magnification image of the upper-half area; (c) the lower-half area of the coating; (d) local high-magnification image of the lower-half area; (e) the middle-junction area of the coating; and (f) local high-magnification image of the junction area.



**Figure 4.** XRD pattern of the CoCrFeNiMo HEA coating prepared through high-speed laser cladding.

### 3.3. Nanoindentation Test Analysis

Nanoscale indentation tests were conducted on the surface of the CoCrFeNiMo high-entropy alloy coating to obtain its micromechanical properties. Figure 5a,b show the contour maps of the coating surface hardness ( $H$ ) and elastic modulus ( $E_r$ ) distribution, respectively. As can be seen from the figures, the contour distributions of the two parameters were relatively similar. With a decrease in the loading force, both the  $H$  and  $E_r$  of the coating increased, which is consistent with the generally accepted principle of materials. The indentation hardness refers to the contact stress of the elastic–plastic contact between the indenter and the test piece, reflecting the ability of the material to resist plastic deformation. The elastic modulus of a material is the ratio of contact stress to contact strain, reflecting the ability of the material to resist elastic deformation. The greater the elastic modulus is, the greater the stiffness of the material.

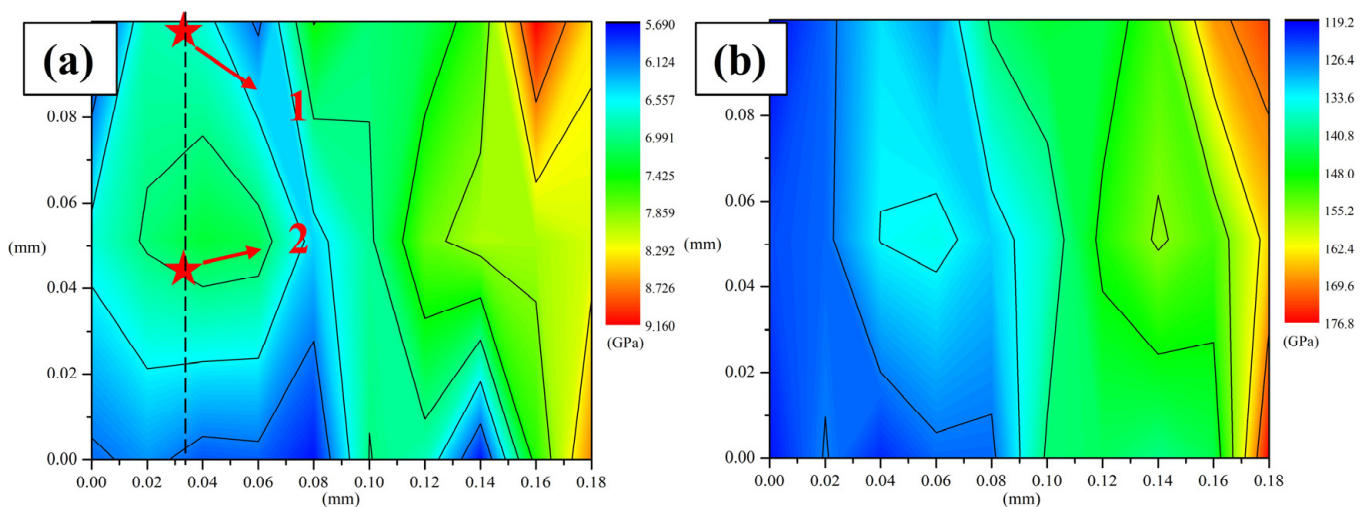


**Figure 5.** Micromechanical property contour maps of the coating surface. (a) Hardness ( $H$ , GPa) contour map and (b) elastic modulus ( $E_r$ , GPa) contour map.

The indentation dots corresponding to points 1 and 2 in Figure 5a had a maximum load of 4000  $\mu\text{N}$ . The hardness (H) values at point 1 and point 2 were measured to be 5.99 and 7.26 GPa, respectively, while the elastic modulus ( $E_r$ ) was determined to be 121.63 and 133.79 GPa, respectively. This implies that the two points signified the two-phase structures inside and outside of the dendrite. The BCC phase was a Mo-rich intermetallic compound exhibiting strong resistance to plastic deformation. Therefore, it could be inferred that point 1 was the FCC structure and that point 2 was the BCC structure.

The time–depth curve and depth–load curve at points 1 and 2 are shown in Figure 6. According to Figure 6a, the deformation processes involved two stages of coating deformation during the loading stage. The first stage was the elastic deformation stage. Under the same uniform loading rate, the strain depth was proportional to the stress, and the deformation degree of the two-phase structures could remain consistent within the elastic deformation limit. The second stage was the plastic deformation stage. As strain accumulated, work hardening occurred, resulting in a decrease in the plastic deformation ability. As can be observed from Figure 6b, the maximum indentation depth at point 2 was notably shallower than that at point 1, suggesting that the interatomic force at point 2 was stronger and had greater resistance to plastic deformation. We calculated the plastic deformation storage energy according to the depth–load curve, with the plastic deformation storage energy values at point 1 and point 2 being  $2.205 \times 10^{-10}$  J and  $1.818 \times 10^{-10}$  J, respectively. Therefore, the FCC structure at point 1 had better fracture toughness. In general, the distribution of the micromechanical properties on the surface of the high-speed laser cladding CoCrFeNiMo HEA coating was uneven, which is consistent with the test results of microhardness. In a word, the micromechanical properties on the surface of high-speed laser cladding CoCrFeNiMo HEA coating displayed an uneven distribution.

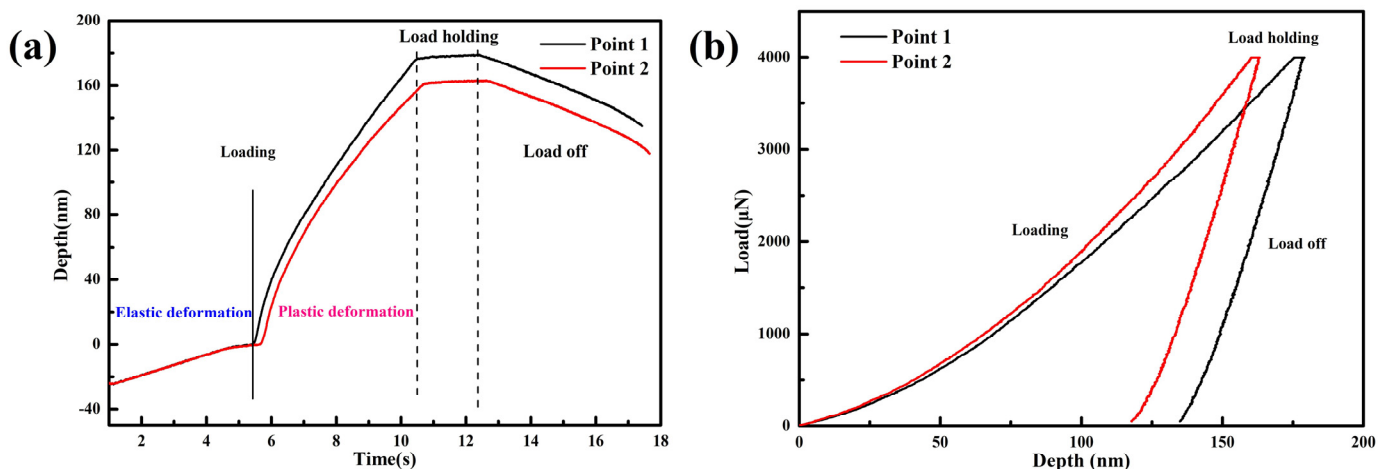


**Figure 6.** Time–depth curves (a) and depth–load curves (b) of the CoCrFeNiMo coating surface when the maximum load is 4000  $\mu\text{N}$ .

### 3.4. Corrosion Resistance Analysis

As shown in Figure 7, the potentiodynamic polarization curve of the high-speed laser cladding CoCrFeNiMo coating is presented. It can be observed that, when the potential  $E$  was between 0.05 and 0.30 V, the coating surface was passivated, and the current decreased slightly with the increasing potential. By employing the Tafel extrapolation technique to fit the potentiodynamic polarization curve, the self-corrosion potential ( $E_{\text{corr}}$ ) and corrosion current density ( $I_{\text{corr}}$ ) of the coating in a 3.5 wt% NaCl solution were determined to be  $-0.362$  V and  $3.69 \times 10^{-6}$  A/cm<sup>2</sup>, respectively.

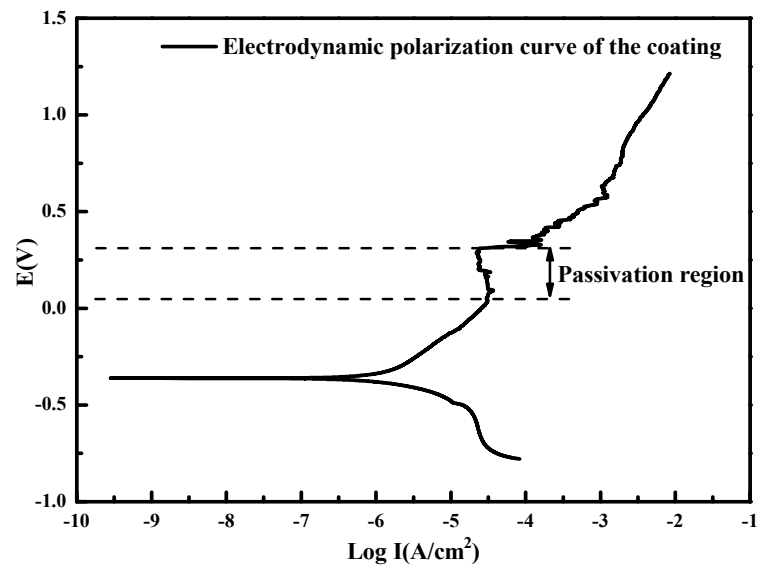


Figure 7. Potentiodynamic polarization curve of the CoCrFeNiMo coating.

Figure 8 shows the impedance spectrum analysis results of the high-speed laser cladding CoCrFeNiMo coating. Figure 8a is the Nyquist plot, and the radius of the capacitive impedance arc indicates the reaction resistance of the coating. The starting point of the real axis  $Z'$  was almost coincident with the origin of the coordinate, suggesting that the solution resistance in the impedance test was almost negligible in comparison with the coating resistance. Additionally, there was a concentration polarization phenomenon at the end of the capacitive impedance arc (low frequency). Figure 8b depicts the Bode plot, where the left longitudinal axis indicates the modulus of impedance  $|Z|$ , and the right longitudinal axis indicates the phase angle. In the low-frequency region,  $|Z|$  was approximately the sum of the charge transfer resistance and the solution resistance. Meanwhile, in the high-frequency region,  $|Z|$  was approximately equal to the solution resistance  $R_s$ , thus demonstrating that the coating resistance was much greater than the solution resistance. In addition, a wide-phase-angle platform can also be observed in Figure 8b, revealing that a relatively stable passivation film was formed during the electrochemical reaction.

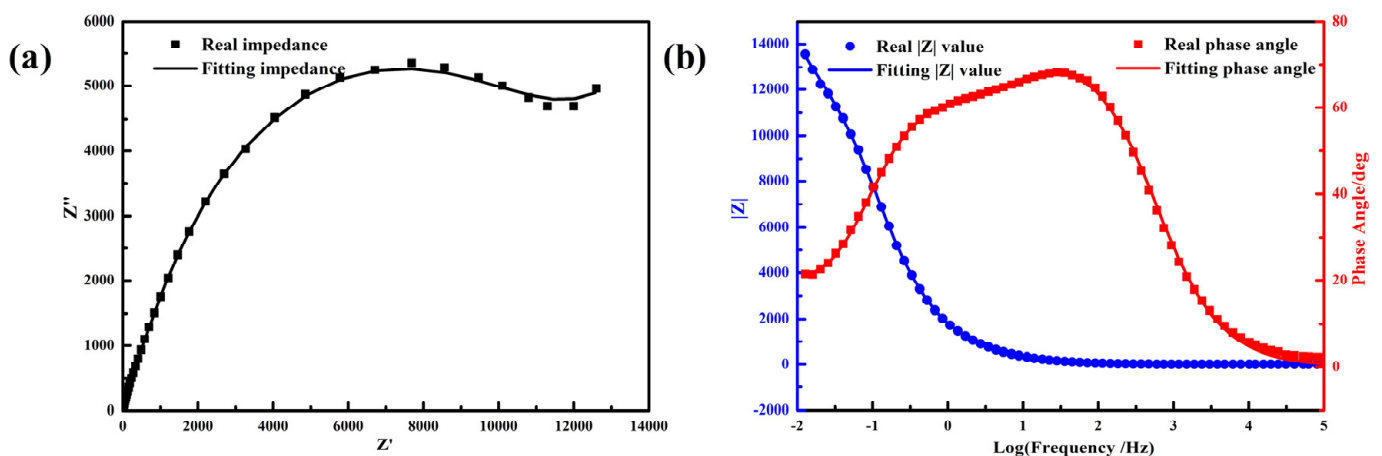
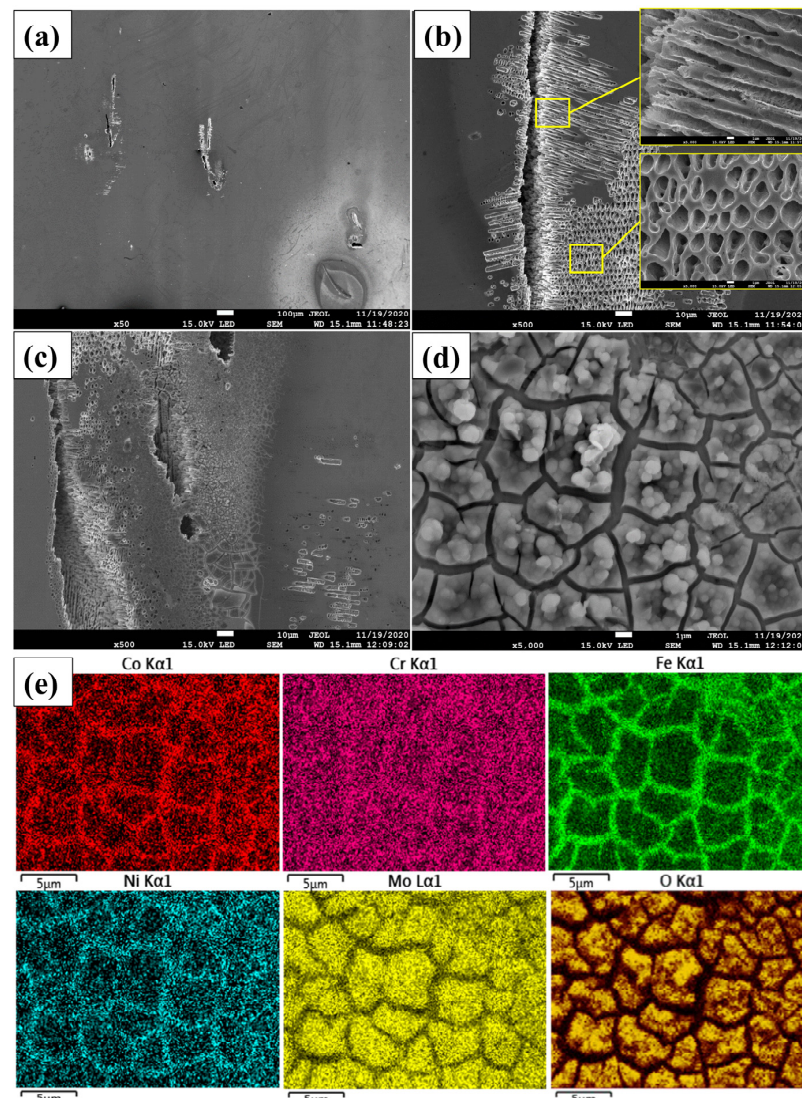


Figure 8. Impedance spectrum analysis results of the CoCrFeNiMo coating. (a) Nyquist plot and (b) Bode plot.

According to the corrosion morphology (Figure 9), the CoCrFeNiMo HEA coating demonstrated only limited localized corrosion in 3.5 wt% NaCl solution, with the corroded area situated at the overlap region. As previously analyzed, the large stress in this region

increased its susceptibility to stress corrosion. The corrosion area was locally enlarged to obtain Figure 9b,c. The corrosion morphology in Figure 9b is similar to that of aqua regia corrosion in Section 3.1. The interdendritic structure (BCC) contained more Mo elements, and its potential was higher than that of the intradendritic structure (FCC), resulting in galvanic corrosion and, consequently, the severe corrosion of the intradendritic structure. Underneath the local corrosion area on the coated surface (as shown in Figure 9c), a cracked film was observed, and Figure 9d is the magnification of Figure 9c. White particles were formed on the film. Figure 9e is the EDS mapping of Figure 9d. According to the mapping diagram, the cracked film was likely to be a passive film composed of O and Mo elements. The potentiodynamic polarization curve indicates that the passive film was broken down when the potential rose above 0.3 V. As Mo is an excellent passivating element, it can induce electrochemical passivation through anodic polarization, forming a dense and solid passivation film, thus significantly enhancing the  $\text{Cl}^-$  corrosion resistance of the coating. Moreover, high-speed laser cladding could significantly refine the grain size of the CoCrFeNiMo HEA coating and create more ion pathways for the formation of a passive film, expediting the formation of a passive film and enhancing the corrosion resistance of the coating.



**Figure 9.** Electrochemical corrosion morphology and mapping results of CoCrFeNiMo coating. (a) Macroscopic corrosion morphology; (b,c) local area images of (a); (d) local area images of (c); and (e) the mapping diagram of (d).

#### 4. Conclusions

In this paper, a CoCrFeNiMo high-entropy alloy coating was fabricated with high-speed laser cladding technology. The microstructure, mechanical properties, and corrosion resistance of the coating were characterized to investigate the effects of the microstructure and composition distribution on the performance of the coating. The following conclusions were drawn.

- (1) The high-speed laser cladding CoCrFeNiMo high-entropy alloy coating had a grain size of only 2~5 microns, with a Mo-rich-phase interdendritic structure with a network distribution. The upper part of the coating was predominantly composed of equiaxed cellular crystals, while the lower part was mostly slender columnar crystals.
- (2) The high-speed laser cladding CoCrFeNiMo coating was composed of both FCC- and BCC-phase structures. Specifically, the intradendritic structure was an FCC phase, while the interdendritic structure was a BCC phase.
- (3) The nanoindentation test results demonstrate that the hardness and elastic modulus of the coating increased as the maximum load decreased. The distribution of the micromechanical properties on the coating surface was not uniform. The BCC-phase structure had a high elastic modulus and superior resistance to deformation, while the softer FCC phase exhibited better fracture toughness. When in the elastic deformation stage, the soft and hard phases could deform cooperatively.
- (4) The coating was subjected to a potentiodynamic polarization test in 3.5 wt% NaCl solution. During anodic polarization, a stable passive film was formed on the coating surface, and local corrosion occurred at the overlap. The self-corrosion potential  $E_{\text{corr}}$  and corrosion current density  $I_{\text{corr}}$  of the coating were  $-0.362$  V and  $3.69 \times 10^{-6}$  A/cm<sup>2</sup>, respectively. The charge transfer resistance of the coating was much higher than solution resistance. High-speed laser cladding could refine the grain of the CoCrFeNiMo high-entropy alloy coating, thus providing more ion pathways for the formation of the passive film, which accelerated the formation of the passive film and enhanced the corrosion resistance of the coating.

**Author Contributions:** Conceptualization, B.H. and Q.Z.; methodology, Q.Z.; validation, M.L.; formal analysis, Q.Z.; resources, M.K.; data curation, F.Q.; writing—original draft preparation, Q.Z.; writing—review and editing, M.L. and Q.W.; visualization, Q.W.; supervision, M.K.; funding acquisition, B.H. and M.L. All authors have read and agreed to the published version of the manuscript.

**Funding:** This research was funded by [National Natural Science Foundation of China] Grant Numbers [51801234] and [51771228]; [Natural Science Foundation of Shandong Province, China] Grant Numbers [ZR2019MEM047]; and [Major Science and Technology Projects of Petro, China] Grant Numbers [ZD2019-184-004]. And The APC was funded by [Major Science and Technology Projects of Petro, China].

**Institutional Review Board Statement:** Not applicable.

**Informed Consent Statement:** Informed consent was obtained from all subjects involved in the study.

**Data Availability Statement:** Data is contained within the article or supplementary material.

**Conflicts of Interest:** The authors declare no conflict of interest.

#### References

1. Steurer, W. Single-phase high-entropy alloys—A critical update. *Mater. Charact.* **2020**, *162*, 110179. [[CrossRef](#)]
2. Sen, S.; Zhang, X.; Rogal, L.; Wilde, G.; Grabowski, B.; Divinski, S.V. ‘Anti-sluggish’ Ti diffusion in HCP high-entropy alloys: Chemical complexity vs. lattice distortions. *Scr. Mater.* **2023**, *224*, 115117. [[CrossRef](#)]
3. He, H.; Lai, M.; Liu, C.; Zeng, G.; He, L.; Zhang, W.; Yi, J.; Liu, S.; Long, J. Effects of deposition temperature on the microstructure, mechanical properties, high temperature corrosion and oxidation properties of AlCrNbTiZr high entropy alloy coatings. *Int. J. Refract. Met. Hard Mater.* **2023**, *112*, 106156. [[CrossRef](#)]
4. Zhang, L.; Cai, W.; Bao, N.; Yang, H. Implanting an Electron Donor to Enlarge the d-p Hybridization of High-Entropy (Oxy)hydroxide: A Novel Design to Boost Oxygen Evolution. *Adv. Mater.* **2022**, *34*, 2110511. [[CrossRef](#)] [[PubMed](#)]

5. Li, W.; Long, X.; Huang, S.; Fang, Q.; Jiang, C. Elevated fatigue crack growth resistance of Mo alloyed CoCrFeNi high entropy alloys. *Eng. Fract. Mech.* **2019**, *218*, 106579. [[CrossRef](#)]
6. Deng, G.; Tieu, A.K.; Lan, X.; Su, L.; Wang, L.; Zhu, Q.; Zhu, H. Effects of normal load and velocity on the dry sliding tribological behaviour of CoCrFeNiMo<sub>0.2</sub> high entropy alloy. *Tribol. Int.* **2020**, *144*, 106116. [[CrossRef](#)]
7. Zhang, Y.; Jiang, X.; Sun, H.; Song, T.; Mo, D.; Li, X.; Luo, Z. Interfacial reaction and microstructure investigation of CoCrFeNiMo medium-entropy alloys diffusion-bonded joints. *Mater. Lett.* **2020**, *274*, 128008. [[CrossRef](#)]
8. Li, K.; Liang, J.; Zhou, J. Microstructure and elevated temperature tribological performance of the CoCrFeNiMo high entropy alloy coatings. *Surf. Coat. Technol.* **2022**, *449*, 128978. [[CrossRef](#)]
9. Zhang, Y.; Jiang, X.; Sun, H.; Shao, Z. Effect of annealing heat treatment on microstructure and mechanical properties of nonequiatomic CoCrFeNiMo medium-entropy alloys prepared by hot isostatic pressing. *Nanotechnol. Rev.* **2020**, *9*, 580–595. [[CrossRef](#)]
10. Wu, W.; Guo, L.; Guo, B.; Liu, Y.; Song, M. Altered microstructural evolution and mechanical properties of CoCrFeNiMo<sub>0.15</sub> high-entropy alloy by cryogenic rolling. *Mater. Sci. Eng. A* **2019**, *759*, 574–582. [[CrossRef](#)]
11. Sui, Q.; Wang, Z.; Wang, J.; Xu, S.; Liu, B.; Yuan, Q.; Zhao, F.; Gong, L.; Liu, J. Additive manufacturing of CoCrFeNiMo eutectic high entropy alloy: Microstructure and mechanical properties. *J. Alloys Compd.* **2022**, *913*, 165239. [[CrossRef](#)]
12. Liu, Y.; Xie, Y.; Cui, S.; Yi, Y.; Xing, X.; Wang, X.; Li, W. Effect of Mo Element on the Mechanical Properties and Tribological Responses of CoCrFeNiMox High-Entropy Alloys. *Metals* **2021**, *11*, 486. [[CrossRef](#)]
13. Karlsdottir, S.N.; Geambazu, L.E.; Csaki, I.; Thorhallsson, A.I.; Stefanoiu, R.; Magnus, F.; Cotrut, C. Phase Evolution and Microstructure Analysis of CoCrFeNiMo High-Entropy Alloy for Electro-Spark-Deposited Coatings for Geothermal Environment. *Coatings* **2019**, *9*, 406. [[CrossRef](#)]
14. Thorhallsson, A.I.; Csaki, I.; Geambazu, L.E.; Magnus, F.; Karlsdottir, S.N. Effect of alloying ratios and Cu-addition on corrosion behaviour of CoCrFeNiMo high-entropy alloys in superheated steam containing CO<sub>2</sub>, H<sub>2</sub>S and HCl. *Corros. Sci.* **2021**, *178*, 109083. [[CrossRef](#)]
15. Csaki, L.; Karlsdottir, S.N.; Stefanoiu, R.; Geambazu, L.E. Corrosion behavior in geothermal steam of CoCrFeNiMo high entropy alloy. *Corrosion* **2018**, *2018*, 11139.
16. Zhicheng, L.; Dejun, K. Microstructure, corrosive-wear and electrochemical properties of laser clad CoCrFeNiMo-B<sub>4</sub>C coatings in 3.5%NaCl solution. *Opt. Laser Technol.* **2023**, *159*, 578–583. [[CrossRef](#)]
17. Qin, G.; Chen, R.; Zheng, H.; Fang, H.; Wang, L.; Su, Y.; Guo, J.; Fu, H. Strengthening FCC-CoCrFeMnNi high entropy alloys by Mo addition. *J. Mater. Sci. Technol.* **2019**, *35*, 578–583. [[CrossRef](#)]
18. Deng, C.; Wang, C.; Chai, L.; Wang, T.; Luo, J. Mechanical and chemical properties of CoCrFeNiMo<sub>0.2</sub> high entropy alloy coating fabricated on Ti6Al4V by laser cladding. *Intermetallics* **2022**, *144*, 107504. [[CrossRef](#)]
19. Qiu, X. Microstructure and mechanical properties of CoCrFeNiMo high-entropy alloy coatings. *J. Mater. Res. Technol.* **2020**, *9*, 5127–5133. [[CrossRef](#)]
20. Du, C.; Hu, L.; Ren, X.; Li, Y.; Zhang, F.; Liu, P.; Li, Y. Cracking mechanism of brittle FeCoNiCrAl HEA coating using extreme high-speed laser cladding. *Surf. Coat. Technol.* **2021**, *424*, 128873. [[CrossRef](#)]
21. Chong, Z.; Sun, Y.; Cheng, W.; Huang, L.; Han, C.; Ma, X.; Meng, A. Laser remelting induces grain refinement and properties enhancement in high-speed laser cladding AlCoCrFeNi high-entropy alloy coatings. *Intermetallics* **2022**, *150*, 107686. [[CrossRef](#)]
22. Lou, L.-Y.; Liu, K.-C.; Jia, Y.-J.; Ji, G.; Wang, W.; Li, C.-J.; Li, C.-X. Microstructure and properties of lightweight Al<sub>0.2</sub>CrNbTiV refractory high entropy alloy coating with different dilutions deposited by high speed laser cladding. *Surf. Coat. Technol.* **2021**, *424*, 127617. [[CrossRef](#)]
23. Chong, Z.; Sun, Y.; Cheng, W.; Han, C.; Huang, L.; Su, C.; Jiang, L. Enhanced wear and corrosion resistances of AlCoCrFeNi high-entropy alloy coatings via high-speed laser cladding. *Mater. Today Commun.* **2022**, *33*, 104417. [[CrossRef](#)]
24. Bae, J.W.; Park, J.M.; Moon, J.; Choi, W.M.; Lee, B.-J.; Kim, H.S. Effect of  $\mu$ -precipitates on the microstructure and mechanical properties of non-equiatomic CoCrFeNiMo medium-entropy alloys. *J. Alloys Compd.* **2019**, *781*, 75–83. [[CrossRef](#)]
25. Ma, X.; Sun, Y.; Cheng, W.; Chong, Z.; Huang, L.; Meng, A.; Jiang, L. Effect of high-speed laser cladding on microstructure and corrosion resistance of CoCrFeNiMo<sub>0.2</sub> high-entropy alloy. *J. Cent. South Univ.* **2022**, *29*, 3436–3446. [[CrossRef](#)]
26. Zhang, Q.; Han, B.; Li, M.; Chen, Z.; Hu, C.; Jia, C. Comparison of CoCrFeNi coatings prepared via high-speed laser cladding and normal laser cladding on microstructure and properties. *Intermetallics* **2023**, *153*, 107795. [[CrossRef](#)]

**Disclaimer/Publisher's Note:** The statements, opinions and data contained in all publications are solely those of the individual author(s) and contributor(s) and not of MDPI and/or the editor(s). MDPI and/or the editor(s) disclaim responsibility for any injury to people or property resulting from any ideas, methods, instructions or products referred to in the content.